Changes in root morphological traits, soil properties, and infiltration characteristics following the conversion of native forests to Carya cathayensis plantations in the Dabie Mountainuous Area, China

YUN ZHU
Nanjing Forestry University
Chunqiang Zhang
Huaihe River Basin Water and Soil Conservation Monitoring Center Station
Yunpeng Wang
Nanjing Forestry University
Hongda Zhang
Huaihe River Basin Water and Soil Conservation Monitoring Center Station
Lei Sun
Nanjing Forestry University
Xia Liu
liuxia@njfu.edu.cn

Nanjing Forestry University
Yanan Wang
Nanjing Forestry University
Abdul Hakim Jamshidi
Nanjing Forestry University
Zhaofei Fan
Auburn University

Research Article

Keywords: Economic forest, Different planting years, Path analysis, Soil erosion, Soil water infiltration

Posted Date: October 6th, 2025

DOI: https://doi.org/10.21203/rs.3.rs-7481786/v1

Additional Declarations: No competing interests reported.

Version of Record: A version of this preprint was published at European Journal of Forest Research on March 5th, 2026. See the published version at https://doi.org/10.1007/s10342-026-01882-w.

Changes in root morphological traits, soil properties, and infiltration characteristics following the conversion of native forests to *Carya cathayensis* plantations in the Dabie Mountainuous Area, China

Yun Zhu[a], Chunqiang Zhang[b], Yunpeng Wang[a], Hongda Zhang[b], Lei Sun[a], Xia Liu[a*], Yanan Wang[a], Abdul Hakim Jamshidi[a], Zhaofei Fan[c]

a. Co-Innovation Center for Sustainable Forestry in Southern China, Jiangsu Province Key Laboratory of Soil and Water Conservation and Ecological Restoration, Nanjing Forestry University, Nanjing, China

b. Huaihe River Basin Water and Soil Conservation Monitoring Center Station, Huaihe River Commission, Bengbu 233001, China

c. College of Forestry, Wildlife and Environment, Auburn University, Auburn, AL 36849, USA

*corresponding author: E-mail address: liuxia@njfu.edu.cn

Abstract: Soil water infiltration is an important hydrological process influencing mountain ecosystems' runoff and soil loss. Our study evaluates soil water infiltration characteristics and the underlying mechanisms under *Carya cathayensis* plantations with different planting years: 6 ($CC_{6\ years}$), 20 ($CC_{20\ years}$), and 50 ($CC_{50\ years}$), and native forest was chosen as control ($CC_{0\ year}$). The Philip, Kostiakov, Kostiakov-lewis, and Horton models were selected to evaluate their applicability under different planting years of *Carya cathayensis* plantations. The results showed that: (1) Converting native forests to *Carya cathayensis* plantations significantly decreased soil water infiltration rates, with average infiltration rate (*AIR*), initial infiltration rate (*IIR*), and stable infiltration rate (*SIR*) decreasing by 33.11% ~ 70.98%, 31.23% ~ 64.11%, and 40.13% ~ 75.01%, respectively；(2) Soil water infiltration rates were improved with planting years, with the highest value shown under $CC_{50\ years}$；(3) The correlation and path analysis indicated that *IIR* and *SIR* were mainly affected by soil non-capillary porosity, while *AIR* was mainly influenced by 5-2 mm water stable aggregate fraction; (4) The Kostiakov model is found to be the most appropriate for characterizing soil infiltration characteristics in the study area. These findings shed insight into soil water infiltration processes and regulating factors for preventing and controlling soil erosion and restoring soil health in land use change, particularly forest cover conversion in the Dabie Mountains area.

Keywords: Economic forest; Different planting years; Path analysis; Soil erosion; Soil water infiltration

1. Introduction

Soil infiltration, which refers to the process of water entering the soil from the land surface, is a crucial hydrological cycle in terrestrial ecosystems, serving as a bridge between groundwater, surface water, and soil water (Lozano-Baez et al., 2019; Wang et al., 2011). Soil infiltration impacts the formation of slope surface runoff, water redistribution, nutrient transport, and soil erosion (Cui et al., 2019; Assouline and Kamai., 2022; Wu et al., 2021). Therefore, studying water infiltration is of great significance for gaining a deeper understanding of soil hydrological processes and preventing soil erosion.

Carya cathayensis, a specific nut tree species in China, provides high-quality nuts and oil product for human beings. Due to large-scale agricultural and forestry development activities since the 1980s, many native forests in the Dabie Mountains area have been extensively converted into *Carya cathayensis* plantations. Land use change has caused adverse impacts on the environment due to the removal of native vegetation (both aboveground and belowground biomass) and slope-based cultivation without soil and water conservation management (Liu et al., 2018; Wu et al., 2013). The soil disturbance during land consolidation, together with the decrease of vegetation canopy and increase of bare soil surface exposed to raindrops, might have caused deterioration of soil properties (Montgomery, 2007; Wang et al., 2017; Zhao et al., 2013). Studies indicated that soil water infiltration rate is significantly influenced by both plant root morphological traits and soil properties (Fischer et al., 2015; Wu et al., 2021; Jia et al., 2017; Molina et al., et al., 2006). *Carya cathayensis* plantations undergo a series of intensive management activities after planting, such as weeding, pruning, and harvesting, which would cause soil compaction and landcover decline. The change in understory vegetation type and diversity will inevitably affect litter input, root morphological traits, and soil properties such as soil porosity, aggregation, organic matter, and bulk density (Kalhoro et al., 2019; Deuchars et al., 1999; Dexter., 2004), thereby would affect the processes of soil water penetration, transportation, and even the regional ecological environment (KODEŠOVÁ et al., 2011; Vizioli et al., 2021;

Taboada et al., 1998).

Planting years were reported to have a direct or indirect effect on soil water infiltration characteristics due to the influence on soil properties and vegetation root distribution in forest ecosystems (Kurmi et al., 2020; Wang et al., 2018b; Das et al., 2018). Long-term planting may lead to an increase in soil compaction and degradation of soil structure, which would cause a decrease in soil infiltration capacity (Wang et al., 2018b; Das et al., 2018). However, other studies pointed out that long-term planting did not necessarily lead to a continuous escalation of soil susceptibility. Vegetation roots gradually developed as increasing planting years and soil organic matter content increased, promoting the formation of soil aggregate structure, which was beneficial for increasing soil porosity and improving soil water infiltration capacity (Jiang et al., 2018; Du et al., 2023). The interconnected soil pores, formed by soil aggregates, regulate the movement and speed of water in the soil through pore structure and properties (Scholl et al., 2014; Chivenge et al., 2011; Wang et al., 2023). Small pores are beneficial for retaining water, whereas larger pores facilitate the movement of water through the soil. In addition, the flow of water in soil pores affects the formation, connectivity, and stability of soil aggregates through the transportation and migration of clay particles; The creation of soil pore networks is fundamentally based on soil aggregates, and their formation process is closely related to root activity (Wu et al., 2021; Liu et al., 2020; Leung et al., 2015).

The typical positive feedback between aggregates and plant roots is as follows: Firstly, plant roots foster aggregate formation through several mechanisms, including the enhancement of wet-dry cycles, exerting physical stress as they grow, secreting phenolic compounds in root exudates, and contributing to the SOM (Jegou et al., 2001; Scholl et al., 2014); Additionally, certain root-associated microorganisms, including soil fungi, can aid in aggregate formation by strengthening the binding between soil particles and small organic compounds (Liu et al., 2015; Luna et al., 2018). Thus, under the background of long-term plantations of *Carya cathayensis*, the alterations in soil water infiltration with changes in plant roots and soil characteristics are influenced by numerous factors over planting time, which is worth further studies.

Establishing a suitable soil infiltration model is crucial for accurately quantifying soil infiltration potential, which is essential for a deeper comprehension of hydrological cyclesand predicting future soil infiltration processes and ecological effects (Liu et al. 2019; Lipiec et al., 2006; Hafiz et al., 2019). Several theoretical models have been proposed to characterize the soil infiltration process (Al-Azawi, 1985; Mao et al., 2011), including the Kostiakov model, the Horton model, the Philip model, and the Kostiakov-Lewis model (Musa and Adeoye., 2010). These models have undergone extensive validation and are commonly applied in field testing and indoor analysis. However, the applicability of soil infiltration models varies in different regions and situations (Mahapatra et al., 2020; Gundalia, 2018; Umar Farid et al., 2019).

This study aimed to examine soil infiltration characteristics under different *Carya cathayensis* planting years ($CC_{6\ years}$, $CC_{20\ years}$, and $CC_{50\ years}$) and select corresponding quantitative models suitable for the Dabie mountainous area. Taking the native forest ($CC_{0\ year}$) as the reference (control), we hypothesized that (i) converting the native forest to *Carya cathayensis* plantations weakened soil infiltrability; (ii) soil infiltrability would be enhanced with the increase of planting years; (iii) the impacts of root morphological traits on soil infiltrability could be contingent upon soil properties. The results will be helpful to the planting and effective management of *Carya cathayensis* for sustainable forest soil and water conservation.

2. Materials and Methods

2.1 Research area

The research area is located in the transition zone between the north and south climates, belonging to the humid monsoon climate of the northern subtropical zone. It is greatly affected by the monsoon, with distinct four seasons, abundant rainfall, concentrated summer rainfall, and significant regional differences and vertical changes. The precipitation is mainly concentrated in summer, with an average annual precipitation of over 1300 mm. Summer rainfall is the most concentrated, accounting for 40% to 50% of the annual precipitation. There are significant spatial differences in rainfall, with more precipitation in mountainous areas compared to hilly areas. The annual average temperature is 15.3 ℃, with an average temperature of 3 ℃ in January and 27.9 ℃ in July. The soil mainly consists of coarse bone soil, yellow brown soil, mountain brown soil, purple soil, and other soil types.

2.2 Experiment design

Carya cathayensis is one of the important economic forest species in Guanmiao Town, Jinzhai County. Prior to the experiment, on-site inspections should be conducted to obtain relevant data from the local government on the establishment and management of *Carya cathayensis* plantations since February 2023. Three different years of *Carya cathayensis* plantations-6 years ($CC_{6\ years}$), 20 years ($CC_{20\ years}$), and 50 years ($CC_{50\ years}$), and a native forest nearby (control) were selected in this study (Fig. 1). Three sampling plots (10 m × 10 m) were set up as replication under each year, and totally 12 sampling plots were employed. The basic information of the sampling plots is summarized in Table 1. Soil management mainly involves weeding and tillage while tree management includes pruning and pecan harvesting. In addition, since the research area is a typical rocky mountainous area with shallow soil layers, the *Carya cathayensis* plantations had a significant impact on the surface soil layer (Zhu et al., 2025). Accordingly, the 0~20 cm soil layer was selected for testing in this study (Niu et al., 2023; Liu et al., 2015).

2.3 Soil sampling and analysis

Soil samples were collected at the vertical projection position of the tree crown projection edge. At each sampling plot, undisturbed soil cores were collected with 100 cm^3 stainless steel cylinders from 0~20 cm soil depth to measure soil water infiltration characteristics, bulk density (BD), and soil porosity. Three undisturbed soils were collected to measure mechanical-stable and water-stable aggregates. To avoid disturbing on soil structure, samples were stored in rigid plastic boxes (17 cm × 11 cm × 7 cm) and carefully delivered to the lab, which were then air-drying immediately and hand-break along natural cracks. Additionally, mixed soil samples were collected with soil auger for analyzing soil organic matter (SOM).

Soil BD, capillary porosity (CP), non-capillary porosity (NCP), and total porosity (TP) were determined using the water suction method (Wang et al., 2008). Briefly, soaking the soil cores (V_t, 100 cm^3) in purified water they reached a consistent weight (m_1) and the water depth did not exceed the bottom cover. Saturating the samples in water for 24 hours until a constant weight (m_2) was obtained. Then, the soil cores were dried at 105 ° C for 24 hours and weighed (m_3). The calculation formulas refer to Eq. (1)-(4):

$$\mathrm{CP} = \frac{m_1 - \mathrm{m}_3}{V_t} \times 100 \tag{1}$$

$$NCP = \frac{m_2 - m_1}{V_t} \times 100 \tag{2}$$

$$TP = CP + NCP \tag{3}$$

$$BD = \frac{m_3}{V_t} \tag{4}$$

Soil organic matter (SOM) was analyzed using the dichromate oxidation method (Bao., 2000). Undisturbed soils were carefully sifted through an 8 mm sieve to measure soil aggregates. The size distribution of mechanical-stable aggregate was measured using dry sieving, and the wet sieving method was used for soil water stable aggregates fractionation with a soil aggregate analyzer (SAA08052, Shanghai) (Su et al., 2010). Soil aggregates stability (including the mean weight diameter (MWD), geometric mean diameter (GMD), and fractal dimension (*D*)) were determined based on Eq. (5)-(7) (Kemper and Rosenau, 1986) to assess the effects of *Carya cathayensis* planting years on the soil structure:

$$MWD = \sum x_i w_i \quad (5)$$

$$GMD = exp\left[\frac{\sum_{i=1}^{n} w_i \times \ln w_i}{\sum_{i=1}^{n} w_i}\right] \quad (6)$$

$$D = 3 - \frac{\log\left(\frac{w_i}{w_0}\right)}{\log\left(\frac{d_i}{d_{max}}\right)} \quad (7)$$

Where: w_0 is the total mass of soil, d_i is the mean diameter of the particle sizes between two sieves, d_{max} is the mean diameter of the largest soil particle size, w_i is the cumulative weight of soil particles smaller than d_i, w_0 is the sum of the weight of each soil particle size, w_i is the mass percentage (%) of the i_{th} particle size aggregate, and x_i refers to the average particle size of the two adjacent size classes (mm).

In practical operation, we attempted to use the double ring method to measure water infiltration in the field. However, due to the large slope of the experimental fields (> 20°), the water surface could not maintain balance, which greatly affected the soil infiltration characteristics data. Secondly, the experiment was conducted in March, and the temperature difference between day and night caused significant changes in soil temperature and humidity throughout the day, significantly affecting water infiltration. Therefore, based on the research of Zhang (2020) and Gan (2023), we chose the indoor cutting infiltration method to measure soil infiltration. An empty ring was placed on top of the collected soil core, the junction sealed with tape and hot wax, and the samples subsequently arranged on a glass funnel with a beaker placed beneath it. Purified water was added into the empty ring placed atop each collected soil core, and timing commenced upon the appearance of the first water drop. The volume of water in the beaker was recorded using a graduated cylinder at intervals of 1, 2, 3, 5, 10, 15 minutes and so on, until three consecutive measurements yielded constant values. Throughout the measurement period, the water level within the ring was maintained at 5 mm by adding purified water as needed, and the water temperature was continuously monitored.

The soil infiltration characteristics were described with three indicators: initial infiltration rate (*IIR*, cm•min^{-1}), stable infiltration rate (*SIR*, cm•min^{-1}), and average infiltration rate (*AIR*, cm•min^{-1}). The *IIR* refers to the infiltration rate before 3 minutes;

The *SIR* is the infiltration rate at which the infiltration amount per unit of time tends to be stable; The *AIR* is the average rate of the entire infiltration process, which is the ratio of the total infiltration amount to the time consumed (Green and Ampt., 1911). The infiltration rate of all soil cores reached stability within 70 minutes.

2.4 Plant root sampling and analysis

Plant roots were obtained with the root drilling method (Ciro et al., 2022). At each sampling plot, 4 soil samples were taken with a soil auger and delivered to the laboratory for root morphological traits measurement. Roots were carefully separated from the soil and repeatedly rinsed with distilled water. Root images were captured with Epson Perfection V750 Photo Scanner and preceded with Win-Rhizo 2009 software to obtain root morphological traits diameter (including average diameter (AD), root length (RL), root surface area (RSA), root length density (RLD), and root volume (RV) (Himmelbauer, Loiskandl, and Kastanek, 2004). Afterward, plant roots were dried at 75°C for 48 h to obtain root biomass (RB) (Liu et al., 2020).

2.5 Soil water infiltration model

$$Horton\ model: A = q + (p - q)\mathrm{e}^{-kt} \tag{8}$$

where A is the infiltration rate (mm·min^{-1}), p is the initial infiltration rate, q is the stable infiltration rate, and k is the empirical parameter (Horton 1940).

$$Philip: A = \frac{1}{2}mt^{-\frac{1}{2}} + n \tag{9}$$

where m is the infiltration coefficient, n is the stable infiltration rate and t is the infiltration time (min). (Dunn and Philip., 1958; Philip, 1957).

$$Kostiakov: A = \alpha\mathrm{t}^{-b} \tag{10}$$

where α and b are empirical parameters, where α is equivalent to the initial infiltration rate. (Naeth et al., 1991; Kostiakov, 1932).

$$Kostiakov - lewis: A = \alpha\mathrm{t}^{-n} + b \tag{11}$$

Where α, b, n are all empirical parameters, where b is equivalent to the stable infiltration rate (Lewis, 1937).

The suitability of these models was assessed through metrics such as the correlation coefficient (*r*), root mean square error (*RMSE*), and coefficient of determination (R^2) based on the simulated and measured data (Nash et al., 1970).

2.6 Statistical analysis

One-way analysis of variance (ANOVA) was conducted to assess differences in soil water infiltration characteristics, root morphological traits, and soil properties among various treatments, while pearson correlation analysis was employed to investigate the relationships among soil water infiltration characteristics, root morphological traits, and soil properties. Stepwise multiple regression analysis was used to select the most important predictors of soil infiltration characteristics. This iterative approach adds or removes variables based on statistical criteria (e.g. *F*- or *t*-tests), resulting in a streamlined model of significant predictors. Based on the regression findings, path analysis partitions each predictor's total effect into direct effects and indirect effects, thus dissect the underlying causal mechanisms. Data were analyzed with SPSS 20.0. The Taylor diagram and infiltration curve fitting were implemented using MATLAB. All results were considered statistically significant if *p-values* were below the 0.05 level.

3. Results

3.1 Soil water infiltration characteristics

Soil infiltration rates decreased sharply within the first 10 mins and then progressively approached stability over time (Fig. 2a). Native forests ($CC_{0\ year}$) had the highest *AIR* (20.54 ($mm \cdot min^{-1}$)), *IIR* (20.03 ($mm \cdot min^{-1}$)), and *SIR* (15.2 ($mm \cdot min^{-1}$)). The conversion of native forests to *Carya cathayensis* plantations decreased the *AIR*, *IIR*, and *SIR* by 33.11%~70.98%, 31.23%~64.11%, and 40.13%~75.01%, respectively. However, with the increase of planting years, the *AIR*, *IIR*, and *SIR* of *Carya cathayensis* plantations increased significantly with the highest soil infiltration rates shown in $CC_{50\ years}$ (Fig.2b, c, and d).

3.2 Soil properties

3.2.1 Soil organic matter, bulk density, and porosity

The conversion of native forests to *Carya cathayensis* plantations significantly increased SOM and BD by 52.63%~97.96% and 22.11%~60%, respectively. Additionally, land use change markedly decreased soil porosity, with the lowest TP shown in $CC_{6\ years}$, followed by $CC_{20\ years}$ and $CC_{50\ years}$. With the increase of planting years, soil BD was significantly decreased, while CP and TP were significantly increased ($p < 0.05$). Soil NCP was not different between *Carya cathayensis* with different planting years. *Carya cathayensis* plantations cultivated for 20 years have the highest SOM, which was 105 $g \cdot kg^{-1}$.

3.2.2 Soil aggregate-size distribution and Stability

The size distribution of mechanical stable aggregates significantly changed after converting native forests to *Carya cathayensis* plantations ($p < 0.05$; Fig.3a). Land use change significantly decreased the proportion of > 5 mm and 5-2 mm aggregate fractions, while increasing the proportion of small aggregate fractions, such as 0.5-0.25 mm fraction, which was 1.5 times higher in $CC_{0\ year}$ than $CC_{6\ years}$ ($p < 0.05$). With the increase of planting years, *Carya cathayensis* plantations significantly decreased the proportions of 0.5-0.25 mm aggregate fractions while increasing the proportions of other fractions ($p < 0.05$; Fig.3a).

The soil mechanical stable aggregates (MWD and GMD) were markedly decreased by land use change. Although soil MWD and GMD were both increased with cultivation years, the values were still significantly lower than that under native forests. (Fig.3b and c). The fractal dimension (*D*) was lowest in $CC_{0\ year}$ and highest in $CC_{6\ years}$. The fractal dimension was gradually decreased with the increasing planting years of *Carya cathayensis*.

The size distribution of water stable aggregates was significantly altered by land use change ($p < 0.05$; Fig. 4a). The < 2 mm aggregate fractions were significantly higher in $CC_{6\ years}$ than $CC_{0\ year}$, while > 2 mm aggregate fractions showed the opposite trend. With the increase of planting years of *Carya cathayensis*, the < 2 mm aggregate fractions tend to decrease while the > 2 mm aggregate fractions tend to increase.

After the native forests were developed into *Carya cathayensis* plantations, the

MWD and GMD of water stable aggregates were decreased to 1/3 and 1/5 in $CC_{6\ years}$ when compared with that in $CC_{0\ year}$, respectively,. The fractal dimension of water stable aggregates in the $CC_{6\ years}$ increased to 2 times of that in the $CC_{0\ year}$ ($p < 0.05$; Fig. 4b, c, and d). Soil MWD and GMD increased, but *D* decreased significantly with the increasing planting years of *Carya cathayensis* ($p < 0.05$).

3.3 Root morphological traits

The root morphological distribution under different treatments was shown in Fig.5a. The RB, RL, AD, RV, RLD and RSA, which were extracted from Fig. 5a, were shown in Fig. 5b, c, d, e, f and g. The ranges were 7.98~33.65 $t{\cdot}hm^{-2}$, 289.87~1420.72 cm, 0.25~0.67 mm, 0.56~4.87 cm^3, 0.29~1.38 $cm{\cdot}cm^{-3}$, and 38.91~289.2 cm^2, respectively. The RB, RL, AD, RV, RLD and RSA all decreased due to land use changes. With the years of *Carya cathayensis* plantation increase, the RB, RL, AD, RV, RLD and RSA were significantly increased ($p < 0.05$). However, even after 50 years of *Carya cathayensis* planting, the values of RB, RL, AD, RV, RLD and RSA in native forests were comparatively higher than those observed.

Correlation analysis showed that root morphological traits were all positively correlated with SOM, CP, NCP, TP, $M_{>5mm}$, $M_{5\text{-}2mm}$, M_{MWD}, M_{GMD}, $W_{>5mm}$, $W_{5\text{-}2mm}$, W_{MWD}, and W_{GMD}, while negatively correlated with BD, M_D, and W_D ($p < 0.05$; Fig.6).

3.4 The correlation between soil infiltration characteristics and environmental factors

The correlation analyses showed that soil infiltration characteristics (*IIR*, *SIR*, and *AIR*) had a significant positive correlation with SOM, CP, NCP, TP, $M_{>5mm}$, $M_{5\text{-}2mm}$, M_{MWD}, M_{GMD}, $W_{>5mm}$, $W_{5\text{-}2mm}$, W_{MWD}, W_{GMD}, RV, RSA, RL, RB, AD and RLD, while a significant negative correlation with BD, M_D, and W_D ($p < 0.05$; Fig.7).

Regression analysis was conducted with *IIR*, *AIR*, and *SIR* selected as dependent variables Y_1, Y_2, and Y_3, respectively, There were a total of 28 factors that were selected as independent variables: SOM (X_1), BD (X_2), CP (X_3), NCP (X_4), TP (X_5), $M_{>5mm}$ (X_6), $M_{5\text{-}2mm}$ (X_7), $M_{2\text{-}1mm}$ (X_8), $M_{1\text{-}0.5mm}$ (X_9), $M_{0.5\text{-}0.25mm}$ (X_{10}), $M_{<0.25mm}$ (X_{11}), M_{MWD} (X_{12}), M_{GMD} (X_{13}), M_D (X_{14}), $W_{>5mm}$ (X_{15}), $W_{5\text{-}2mm}$ (X_{16}), $W_{2\text{-}1mm}$ (X_{17}), $W_{1\text{-}0.5mm}$ (X_{18}), $W_{0.5\text{-}0.25mm}$ (X_{19}), W_{MWD} (X_{20}), M_{GMD} (X_{21}), M_D (X_{22}), RV (X_{23}), RSA (X_{24}), RLD (X_{25}), RL (X_{26}), AD (X_{27}), and RB (X_{28}). Multivariate stepwise regression identified the key and independent factors affecting soil *IIR*, *AIR,* and *SIR*. Further path analysis was conducted to assess their direct and indirect impacts on the extent of soil infiltration.

The coefficients of R^2 for soil *IIR*, *AIR*, and *SIR* were 0.992, 0.981, and 0.993, respectively (Table 3). Regression analysis indicated a substantial relationship among the variables, and the resulting model had statistical significance. At the same time, the stepwise multiple regression revealed that soil BD, NCP, $W_{5\text{-}2mm}$, and RB were the primary determinants influencing soil infiltration characteristics (*IIR*, *AIR*, and *SIR*) in the study area. In order to determine the degree of influence of the selected factors on soil infiltration rates, path analysis was conducted.

Soil NCP, $W_{5\text{-}2mm}$, and RB had direct positive impacts on *IIR*, *SIR*, and *AIR*, while BD had a direct negative impact on infiltration characteristics (Table 4). The direct influencing factors of water infiltration characteristics were NCP and $W_{5\text{-}2mm}$. The overall indirect influence of BD and RB on soil infiltration characteristics exceeded their direct effects, and the indirect effects affected soil water infiltration characteristics mainly through NCP and $W_{5\text{-}2mm}$. According to the determination coefficients in Fig. 8, the factors affecting *IIR* and *SIR* followed the order: NCP > $W_{5\text{-}2mm}$ > BD > RB, while the ranking of factors affecting the *AIR* was $W_{5\text{-}2mm}$ > NCP > BD > RB.

3.5 Fitting and accuracy evaluation of soil infiltration models

Correlation coefficient (*r*), root mean square error (RMSE), coefficient of determination (R^2), standard deviation, and empirical parameters were used to evaluate the applicability of four infiltration models in simulating soil infiltration processes under different planting years. In the Taylor diagram, each model is plotted as a point, and the closer that point lies to the observational reference, the greater the overall agreement in correlation, variability, and precision. According to the statistical parameters simulated by different infiltration models (Fig. 9), it can be seen that all four infiltration models can simulate the infiltration process of soil under different planting years well, with a correlation coefficient between 0.85 and 1.00 and a determination coefficient ≥ 0.84. Among them, the Kostiakov model has the highest *r* (> 0.95), R^2 (> 0.91), and minimum RMSE value at different experimental points (Fig. 10 and Table 5), indicating that the Kostiakov model is most suitable for simulating the infiltration process, while Philip model was poor (with the lowest *r* and standard deviation, and the highest RMSE). In the Kostiakov-Lewis model, the *b*-value represents *SIR*, and the simulation results were intermediate between -37.740 and 3.709. The *b*-values of $CC_{0\ year}$, $CC_{20\ years,}$ and $CC_{50\ years}$ were negative, inconsistent with the actual infiltration theory (Table 5). In summary, the Kostiakov model is the most suitable for describing the infiltration process under different planting years in *Carya cathayensis* plantation.

4. Discussion

4.1 Soil infiltration characteristics as affected by land use change

Changes in land use can alter stand structure, understory vegetation diversity, and soil structure, thereby affecting soil water infiltrability (Wang et al., 2018a; Fischer et al., 2015). In this study, converting the native forests to *Carya cathayensis* plantations significantly decreased soil infiltration characteristics (Fig. 2). This result was consistent with previous findings regarding the effects of land use change on soil infiltration capacity (Neris et al., 2012; Ma et al., 2007). According to the field survey, there was higher vegetation coverage, litter, and thicker humus layer under native forests than *Carya cathayensis* plantation (Table 1). Vegetation coverage and litter could intercept rainfall in the vertical direction and block slope runoff in the horizontal direction (Li et al., 2016; Himmelbauer et al., 2004). At the same time, the higher amount of litter would lead to a higher soil organic matter content, which fosters soil aggregates, further improving soil structure, increasing soil porosity, and enhancing soil water infiltration performance to avoid soil erosion (Sun et al., 2018; Yimer et al., 2008; Tu et al., 2023). The composition of plant species under *Carya cathayensis* plantation is relatively simple due to land management, such as weeding might lead to a drastic decline in aggregate stability in the soils after planting *Carya cathayensis* (Table 1, Fig.3 and 4). We found that some of the large aggregates (> 2 mm) are destroyed to form smaller aggregates after land use change which would easily lost with surface runoff (Fig.3 and 4), consistent with Casermeiro et al. (2004) and Bruno et al. (2021). Meanwhile, soil compaction (higher BD under *Carya cathayensis* plantation) caused by harvest activity would destroy the soil aggregation structure, change the number and size of large pores, make the soil denser, and weaken the water permeability (Watanabe et al., 2017). Additionally, the formed small soil aggregates by destroying large aggregates ($W_{5\text{-}2mm}$) might block large pores to hinder water penetration (Gong et al., 2018). The dispersed clay particles may also form a dense layer on the soil surface, decreasing infiltration capacity (Wu et al., 2016a). Our result demonstrated that soil infiltration characteristics were correlated with CP, NCP, TP, SOM, $M_{>5mm}$, $M_{5\text{-}2mm}$,

M_{MWD}, M_{GMD}, $W_{>5mm}$, $W_{5\text{-}2mm}$, W_{MWD}, and W_{GMD}, similar to Zhong et al (2017) and KODEŠOVÁ R et al (2011) ($p < 0.05$; Fig. 8). It is generally believed that soil organic matter can promote the formation of soil aggregate structure, increase the stability of aggregates, improve soil pore structure, and thereby promote soil water infiltration (Mailapalli 2012; Edmondson et al., 2014; Wu et al., 2021).

It is worth noting that our findings showed that forest soils exhibit infiltration rates 2~4 times higher than those in agricultural or grassland systems under different land use types, consistent with observations by Wilpert (2022). The enhanced infiltration in forested terrain primarily results from:1) surface cover, such as litter layers and understory vegetation, which buffer raindrop impact, reduce compaction, and enable more effective water entry (Kalhoro et al., 2019); 2) extensive root systems, especially mature tree roots, which create stable macropores that act as rapid water conduits into the soil profile (Ghestem et al., 2011; Zhao et al., 2013). Yet high infiltration does not automatically eliminate erosion risk. In our study area, short-term, high-intensity rainfall during the plum-rain (June~July) and typhoon (July~September) seasons can temporarily surpass infiltration capacity, particularly on bare or disturbed surfaces. Under such conditions, slope gradient, vegetation cover, surface sealing, and antecedent soil moisture interact to influence runoff and erosion potential. For example, steep slopes shorten residence time for surface water, increasing overland flow risk; shallow soils or exposed bedrock restrict vertical infiltration and encourage lateral subsurface flow. Meanwhile, the infiltration rates measured in this study were derived under controlled laboratory conditions, where surface heterogeneity and compaction are minimized. Field conditions often feature crust formation, variable surface roughness, or localized compaction, which can reduce actual infiltration efficiency.

4.2 Soil infiltration characteristics as affected by planting years of *Carya cathayensis* plantations

Changes in planting years alter understory vegetation diversity, litter, and root morphological traits, resulting in changes in soil porosity, aggregates, organic matter, and soil bulk density, which in turn affect soil infiltrability (Vizioli et al., 2021; Vivoni et al., 2008; Zheng et al., 2022). Our study showed that long-term (> 50 years) planting of *Carya cathayensis* improved soil structure, the finding aligned with the results reported by Wu et al. (2013). The increased MWD and GMD enhanced its erosion resistance, which benefits soil infiltration characteristics (Fig. 2, 3, and 4). Compared to the old *Carya cathayensis* forests, the newly planted *Carya cathayensis* forests had more human cultivation operations, such as pesticide application and continuous use of heavy machinery, which leads to soil compaction and degradation, thereby reducing soil water infiltration. However, Sone et al. (2019) demonstrated that long-term continuous cropping degrades soil hydraulic properties by compromising aggregate structure, reducing porosity, and depleting organic matter. These effects are intensified by diminished root density and litter inputs in croplands relative to agroforestry systems. This mechanistic pathway—structural deterioration due to biogenic resource loss—underpins the observed reductions in soil water infiltration characteristics. With the increase of planting years, the canopy in the *Carya cathayensis* plantations increased gradually, and plant residues (litter) and also increased (Table 1; Fig. 5 and 6). Larger canopy can intercept more rainwater, buffer the impact of rainwater on the soil, avoid the destruction of soil aggregate structure, and reduce soil erosion (Tu et al., 2023; Noellemeyer et al., 2008). In addition, plant roots also have an impact on soil *IIR*, *AIR*, and *SIR* (Ghestem et al., 2011; Zhao et al., 2013; Leung et al., 2018), which was supported by our results (Fig. 7). The root system serves as the main pathway for the material connection between soil and plants, and the main initial source of soil organic matter (Cui et al., 2019; Zhao et al., 2013; Wu et al., 2021), as supported by a significant positive correlation between plant roots and SOM (Fig.6; Wu et al., 2016a; Guo et al., 2019b). Root residues could increase SOM, fostering soil aggregates and improving soil porosity and aeration (Zhang et al., 2019). Therefore, the increased root with time provided more binding agent to form aggregates, thereby increasing soil aggregate stability and porosity (Table 2; Fig.3 and 4), and correspondingly enhancing water infiltration capacity (Fig.6; Poulenard et al., 2001; Zhu et al., 2020).

Path analysis indicated that soil BD, NCP, $W_{5\text{-}2mm}$, and RB are the main influencing factors, directly or indirectly affected soil *IIR*, *AIR*, and *SIR* (Table 4). The physical entanglement effect of roots in soil caused entanglement and rearrangement of soil particles, would lead to changes in soil aggregate structure (Huang et al., 2017; Bronick and Lal., 2005). The macroaggregates are mainly formed by the entanglement and cementation of microbial secretions and organic binders (Guo et al., 2019a; Elliott, E., 1986). With the increase of the content of $W_{5\text{-}2mm}$, when raindrops hit the soil, the dispersion and damage rate of water stable aggregates decreased, and soil stability aggregates were enhanced. The stronger the soil's erosion resistance, the more favorable it was for water infiltration (Gong et al., 2018; KODEŠOVÁ R et al., 2011). We found that NCP had a more direct impact on soil infiltrability, similar to the results reported by Kabir et al (2020) and Wu et al (2016b). The decay of the root system changed the soil pore structure of the soil (Leung et al., 2015; Sun et al., 2018; Hudek et al., 2010). With the increase in soil NCP, the longitudinal and transverse water infiltration rates in the soil significantly increased, and the infiltration time was relatively short, which provided a good premise for soil water infiltration within a certain range (Jiang et al., 2018; Bronick and Lal, 2005; Jørgensen et al., 2002).

4.3 Evaluation of the Applicability of Infiltration Models

Compared with most models that only use the coefficient of determination (R^2) or other single overall goodness of fit evaluation indicators to evaluate the goodness of fit, this study simultaneously uses correlation coefficient (r), root mean square error (RMSE), and standard deviation to verify and evaluate the simulation goodness of fit and the adaptability of each model. The nonlinear regression analysis indicated that the Kostiakov-lewis and Kostiakov models had better fitting effects. The Kostiakov model had the highest prediction accuracy and was deemed the most appropriate for simulating the water infiltration process (Table 5; Fig. 9 and 10), consistent with Silva's research results (2007). The Kostiakov model belongs to the empirical model, and the model parameters have no clear physical meaning. Its simple model form can effectively describe the short-term infiltration process, which is the case for our experiment. However, the Kostiakov-lewis model has higher prediction accuracy for long-term water infiltration (Silva., 2007). In addition, Philip model is a physical model that generally has a good fitting effect on the one-dimensional infiltration of homogeneous soil. In contrast, the Horton model takes actual infiltration values for simulation, which is less applicable than the Kostiakov model due to the influence of soil structure (Flerchinger. et al., 2006). On the contrary, Madab et al (2019) showed that the Kostiakov and Philip models had the lowest accuracy in predicting water infiltration before and after rice planting. This is mainly because the selected soil infiltration models are all derived under specific applicable conditions, which, to some extent, reflect the infiltration laws and do not have universal applicability. Future attention should be paid to studying soil infiltration processes in different regions and research objects.

5. Conclusion

Land use change from native forests to *Carya cathayensis* plantations decreased soil water infiltration characteristics, which supports our first hypothesis. The decreased infiltration performance was due to the decreased proportion of >2 mm aggregate fractions, NCP and RB, and increased BD. With the increase of planting years, soil infiltrability would be enhanced as the formation of large aggregates, the decreased soil compaction, the improved soil aggregate stability, and enhanced root biomass, which might be beneficial for preventing soil erosion. Soil NCP and $W_{5\text{-}2mm}$ were the predominant factors directly influencing soil infiltrability. Root affected soil infiltrability primarily through NCP and $W_{5\text{-}2mm}$ which support our third hypothesis. Soil properties exerted a more significant influence on soil water infiltration capacity compared to root system characteristics, and the NCP and $W_{5\text{-}2mm}$ can be selected as indicators for evaluating and analyzing the soil infiltration characteristics of *Carya cathayensis* plantations in the Dabie Mountains area. The most suitable soil infiltration model for our research area is the Kostiakov model, succeeded closely by the Horton model.

CRediT authorship contribution statement

Declaration of Competing Interest

The authors confirm that they have no competing financial interests or personal affiliations that might be perceived as influencing the research presented in this paper.

Data availability

Data will be provided on request.

Acknowledgments

We are grateful for the support provided by the National Natural Science Foundation of China (32071840 and 31070627), the National Key Research and Development Program of China (2018YFC0507005), the Postgraduate Research & Practice Innovation Program of Jiangsu Province (KYCX24_1260), and the Jiangsu Provincial Government Scholarship for Studying Abroad during this investigation. We would also grateful to all project sponsors and reviewers for their valuable feedback.

Reference:

Al-Azawi S A., 1985. Experimental evaluation of infiltration models. J. Hydrol. 24(2), 77–88. http://www.jstor.org/stable/43944562.

Assouline, S., Kamai. T., 2022. Unique relationship between rate and cumulative flow: A property of infiltration and evaporation in soils.Geophysical Research Letters, (6), 49. https://doi.org/ 10.1029/2021GL097449

Bao, S. D., 2000. Soil and agricultural chemistry analysis (in Chinese). Beijing, China: China Agriculture Press.

Bronick, C.J., Lal, R., 2005. Soil structure and management: a review. Geoderma. 124(1), 3–22. https://doi.org/ 10.1016/j.geoderma.2004.03.005.

Casermeiro, M.A., Molina, J.A., de la Cruz Caravaca, M.T., et al., 2004. Influence of scrubs on runoff and sediment loss in soils of Mediterranean climate. Catena. 57(1), 91–107. https://doi.org/ 10.1016/S0341-8162(03)00160-7

Chivenge, P., Vanlauwe, B., Gentile, R., et al., 2011. Organic resource quality influences short-term aggregate dynamic sand soil organic matter and nitrogen accumulation. Soil Biol Biochem. 43(3), 657 – 666. https://doi.org/ 10.1016/j.soilbio.2010.12.002

Ciro, C., Laura, T.R., Neus, M.M., et al., 2022. Comparing two field protocols to measure individual shrubs' root density distribution. Plant Soil. 481(1-2), 691-699. https://doi.org/10.1007/S11104-022-05657-1

Cui, Z., Wu, G.L., Huang, Z., et al., 2019. Fine roots determine soil infiltration potential than soil water content in semi-arid grassland soils. J. Hydrol. 578, 124023. https://doi.org/ 10.1016/j.jhydrol.2019.124023

Das, A., Lyngdoh, D., Ghosh, P.K., 2018. Tillage and cropping sequence effect on physico–chemical and biological properties of soil in Eastern Himalayas. India. Soil Tillage Res. 180, 182–193. https://doi.org/10.1016/j.still.2018.03.005

Dexter, R.A. 2004. Soil physical quality Part I. Theory, effects of soil texture, density, and organic matter, and effects on root growth. Geoderma. 120(3-4), 201–214. https://doi.org/ 10.1016/j.geoderma.2003.09.004.

Deuchars, S.A., Townend, J., Aitkenhead, M.J., et al., 1999. Changes in soil structure and hydraulic properties in regenerating rain forest. Soil Use Manage. 15(3), 183-187. https://doi.org/ 10.1111/j.1475-2743.1999.tb00086.x

Du, X.J., Hu, H., Wang, T.H., Zou, L., Zhou, W.F., 2023. Long–term rice cultivation increases contributions of plant and microbial–derived carbon to soil organic matter in saline–sodic soils. Sci. Total Environ. 904, 16671. https://doi.org/10.1016/j.scitotenv.2023.166713

Dunn, G.H., Phillips, R.E., 1958. Macroporosity of a well-drained soil under no-till and conventional tillage. Soil Sci SOM Am J. 55(3), 817–823. https://doi.org/ 10.2136/sssaj1991.03615995005500030031x

Edmondson, J.L., O'Sullivan, O.S., Inger, R., et al., 2014. Urban tree effects on soil organic matter. PLoS One. 9(7), e101872. https://doi.org/ 10.1371/journal.pone.0101872

Elliott, E., 1986. Aggregate structure and carbon, nitrogen, and phosphorus in native and cultivated soils. Soil Sci. SOM. of Am. J. 50(3), 627-633. https://doi.org/ 10.2136/sssaj1986.03615995005000030017x

Flerchinger, G.N., Seyfried, M.S., Hardegree, S.P., 2006. Using soil freezing characteristics to model multi-season soil water dynamics. Vadose Zone J. 5(4), 1143-1153. https://doi.org/ 10.2136/vzj2006.0025

Fischer, C., Tischer, J., Roscher, C., et al., 2015. Plant species diversity affects infiltration capacity in an experimental grassland through changes in soil properties. Plant Soil. 397(1-2), 1–16. https://doi.org/ 10.1007/s11104-014-2373-5

Gan, F.L., Shi, H.L., Gou, J.F., et al. 2023. Effects of bedrock strata dip on soil infiltration capacity under different land use types in a karst trough valley of Southwest China. Catena. 230. https://doi.org/10.1016/J.CATENA.2023.107253

Ghestem, M., Sidle, R.C., Stokes, A., 2011. The influence of plant root systems on subsurface flow: Implications for slope stability. Biosci. 61(11), 869–879. https://doi.org/ 10.1525/bio.2011.61.11.6

Gong, Y., Tian, R., Li, H., 2018. Coupling effects of surface charges, adsorbed counterions and particle - size distribution on soil water infiltration and transport. Eur. J. Soil Sci. 69(6), 1008-1017. https://doi.org/ 10.1111/ejss.12721

Guo, L., Liu, Y., Wu, G.L., et al., 2019a. Preferential water flow: Influence of alfalfa (Medicago sativa L.) decayed root channels on soil water infiltration. J. Hydrol. 578, 124019.

https://doi.org/ 10.1016/j.jhydrol.2019.124019
Guo, Z., Zhang, L., Yang, W., et al., 2019b. Aggregate Stability under Long-Term Fertilization Practices: The Case of Eroded Ultisols of South-Central China. Sustainability. 11(4), 1169. https://doi.org/ 10.3390/su11041169
Gundalia, M., 2018. Estimation of infiltration rate based on complementary error function peak for Ozat watershed in Gujarat (India). Int. J. Hydrol. 2(3), 289-294. https://doi.org/ 10.15406/ijh.2018.02.00083
Green, W.H., Ampt, G.A., 1911. Studies on Soil Phyics. J. Agric. Sci. 4, 1–24. https://doi.org/ 10.1017/S0021859600001441
Horton, R.E, 1940. An approach towards physical interpretation of infiltration capacity. Proc Soil Sci SOM Am. 5, 399–417. https://doi.org/ 10.2136/sssaj1941.036159950005000C0075x
Hafiz, F.U., Zahid, K.M., Ijaz, A., et al., 2019. Estimation of infiltration models parameters and their comparison to simulate the onsite soil infiltration characteristics. Int. J. Agric. Biol. Eng. 12(3), 84-91. https://doi.org/ 10.25165/j.ijabe.20191203.4015
Himmelbauer L M ,Loiskandl W ,Kastanek F., 2004. Estimating length, average diameter and surface area of roots using two different Image analyses systems. Plant Soil, 260(1-2), 111-120. https://doi.org/10.1023/B:PLSO.0000030171.28821.55
Huang, Z., Tian, F.P., Wu, G.L., et al., 2017. Legume grasslands promote precipitation infiltration better than gramineous grasslands in arid regions. Land Degrad. Dev. 28(1), 309–316. https://doi.org/ 10.1002/ldr.2635
Hudek, C., Burylo, M., Rey, F., 2010. Root system traits of Mahonia aquifolium and its potential use in soil reinforcement in mountain horticultural practices. Sci. Hortic. 125(3), 504-511. https://doi.org/ 10.1016/j.scienta.2010.04.035
Jegou, D., Schrader, S., Diestel, H., et al., 2001. Morphological, physical and biochemical characteristics of burrow walls formed by earthworms. Applied Soil Ecology. 17(2), 165-174. https://doi.org/ 10.1016/S0929-1393(00)00136-0
Jia, X.X., Shao, M.A., Zhu, Y.J., et al., 2017. Soil moisture decline due to afforestation across the Loess Plateau China. J. Hydrol. 546, 113–122. https://doi.org/10.1016/j. jhydrol.2017.01.011.
Jiang, X.J., Liu, W.J., Chen, C.F., et al., 2018. Effects of three morphometric features of roots on soil water flow behavior in three sites in China. Geoderma, 320, 161-171. https://doi.org/

10.1016/j.geoderma.2018.01.035

Jørgensen, P.R., Hoffmann, M., Kistrup, J.P., et al., 2002. Preferential flow and pesticide transport in a clay-rich till: field, laboratory, and modeling analysis. Water Resour Res. 38(11), 1246–1261. https://doi.org/ 10.1029/2001WR000494.

Kabir, E.B., Bashari, H., Bassiri, M., et al., 2020. Effects of land-use/cover change on soil hydraulic properties and pore characteristics in a semi-arid region of central Iran. Soil Tillage Res. 197, 104478. https://doi.org/ 10.1016/j.still.2019.104478

Kalhoro, S.A., Ding, K., Zhang, B., et al., 2019. Soil infiltration rate of forestland and grassland over different vegetation restoration periods at Loess Plateau in northern hilly areas of China. Landsc Ecol Eng. 15(1), 91-99. https://doi.org/ 10.1007/s11355-018-0363-0

Kemper, W.D., Rosenau, R.C., 1986. Aggregate stability and size distribution. Methods of Soil Analysis. Part 1, 2nd ed. Am. SOM. Agron., Madison. 425–442. https://doi.org/ 10.2136/sssabookser5.1.2ed.c17

Kodešová R., Jirků V., Kodeš V., et al., 2011. Soil structure and soil hydraulic properties of Haplic Luvisol used as arable land and grassland. Soil Tillage Res. 111(2), 154-161. https://doi.org/ 10.1016/j.still.2010.09.007

Kostiakov, A.N., 1932. On the dynamics of the coefficient of water-percolation in soils and on the necessity of studying it from a dynamic point of view for purposes of amelioration. Trans. 6th Comm. Int. SOM. Soil Sci. Russian. 17–21.

Kurmi, B., Nath, J.A., Lal, R., et al., 2020. Water stable aggregates and the asSOMiated active and recalcitrant carbon in soil under rubber plantation. Sci Total Environ. 703(C), 135498. https://doi.org/ 10.1016/j.scitotenv.2019.135498

Leung, A.K., Garg, A., Coo, J.L., et al., 2015. Effects of the roots of Cynodon dactylon and Schefflera heptaphylla on water infiltration rate and soil hydraulic conductivity. Hydrol.

Process. 29(15), 3342–3354. https://doi.org/ 10.1002/hyp.10452
Leung, A.K., Boldrin, D., Liang, T., et al., 2018. Plant age effects on soil infiltration rate during early plant establishment. Géotechnique. 68(7), 646–652. https://doi.org/ 10.1680/JGEOT.17.T.037
Lewis, M.R., 1937. The rate of infiltration of water in irrigation-practice. Eos. Trans. Am. Geophys. Union. 18(2), 361–368. https://doi.org/ 10.1029/TR018i002p00361
Li, H., Shen, H.H., Chen, L.Y., et al., 2016. Effects of shrub encroachment on soil organic matter in global grasslands. Sci. Rep. 6(1), 28974.
Lipiec, J., Ku´s, J., Słowinska-Jurkiewicz, ´A., et al., 2006. Soil porosity and water infiltration as influenced by tillage methods. Soil Tillage Res. 89(2), 210–220. https://doi.org/ 10.1016/j.still.2005.07.012
Liu, Y., Guo, L., Huang, Z., et al., 2020. Root morphological characteristics and soil water infiltration capacity in semi-arid artificial grassland soils. Agric Water Manag. 235, 106153. https://doi.org/ 10.1016/j.agwat.2020.106153
Liu, B., Xie, G., Zhang, X., et al., 2015. Vegetation root system, soil erosion and ecohydrology system: A review. International Forum on Energy, Environment Science & Materials. https://doi.org/ 10.2991/ifeesm-15.2015.52.
Liu, Y., Cui, Z., Huang, Z., et al., 2019. Influence of soil moisture and plant roots on the soil infiltration capacity at different stages in arid grasslands of China. Catena. 182, 104147. https://doi.org/ 10.1016/j.catena.2019.104147
Liu, Y., Miao, H.T., Huang, Z., et al., 2018. Soil water depletion patterns of artificial forest species and ages on the Loess Plateau (China). For. Ecol. Manage. 417, 137–143. https://doi.org/ 10.1016/j.foreco.2018.03.005.
Liu, L. C., Wu, Z.Y., Liu, J.Q., 2015. Effects of land use on spatial patterns of soil properties in a rocky mountain area of Northern China. Arab. J. Geosci, 8(2), 1181-1194. https://doi.org/ 10.1007/s12517-013-1233-6.
Lozano-Baez, S.E., Cooper, M., Meli, P., et al., 2019. Land restoration by tree planting in the tropics and subtropics improves soil infiltration, but some critical gaps still hinder conclusive results. For. Ecol. Manage. 444, 89–95. https://doi.org/ 10.1016/j.foreco.2019.04.046
Luna, L., Vignozzi, N., Miralles, I., et al., 2018. Organic amendments and mulches modify soil

porosity and infiltration in semiarid mine soils. Land Degrad. Dev. 29, 1019–1030. https://doi.org/ 10.1002/ldr.2830

Ma, X., Zhang, B., Shi, D., et al., 2007. Study on soil infiltration characteristic of different land utilization types in purple soil hilly region. J. Soil Water Conserv. 21, 25–29. https:// 10.13870/j.cnki.stbcxb.2007.05.005

Mahapatra, S., Jha, M.K., Biswal, S., et al., 2020. Assessing Variability of Infiltration Characteristics and Reliability of Infiltration Models in a Tropical Subhumid Region of India. Sci. Rep. 10(1), 1515. https://doi.org/ 10.1038/s41598-020-58333-8

Madab, K., Mahapatra, S., Mohan, C., et al. 2019. Infiltration characteristics of lateritic vadose zones: Field experiments and modeling. Soil Till Res. 18(7), 219-234. https://doi.org/ 10.1016/j.still.2018.12.007

Mailapalli, D.R., Horwath, W.R., Wallender, W.W., et al., 2012. Infiltration, runoff, and export of dissolved organic matter from furrow-irrigated forage fields under cover crop and no-till management in the Arid Climate of California. J. Irrig Drain Eng. 138(1), 35-42. https://doi.org/ 10.1061/(ASCE)IR.1943-4774.0000385.

Mao, L.L., Lei, T.W., Bralts, V.F., 2011. An analytical approximation method for the linear source soil infiltrability measurement and its application. J. Hydrol. 411(3), 169–177. https://doi.org/ 10.1016/j.jhydrol.2011.08.066

Molina, A., Govers, G., Poesen, J., et al., 2006. Environmental factors controlling spatial variation in sediment yield in a central Andean mountain area. Geomorphology. 98(3), 176-186. https://doi.org/ 10.1016/j.geomorph.2006.12.025

Montgomery, D.R., 2007. Soil erosion and agricultural sustainability. Proceedings of the National Academy of Sciences of the United States of America, 104(33), 13268-13272. https://doi.org/10.1073/pnas.0611508104

Musa, J.J., Adeoye, P.A., 2010. Adaptability of Infiltration Equations to the Soils of the Permanent Site Farm of the Federal University of Technology, Minna, in the Guinea savannah zone of Nigeria. Au J. Tech. 2(14), 147-155.

Nash, J.E., Sutcliffe, J.V., 1970. River flow forecasting through conceptual models part I — A discussion of principles – Science Direct. J. Hydrol. 10(3), 282-290. https://doi.org/ 10.1016/0022-1694(70)90255-6

Naeth, M.A., Chanasyk, D.S., BaileyA, W., 1991. Applicability of the Kostiakov equation to mixed prairie and fescue grasslands of Alberta. J. Range Manag. 44(1), 18–21. https://doi.org/ 10.2307/4002631

Neris, J., Jiménez, C., Fuentes, J., et al., 2012. Vegetation and land-use effects on soil properties and water infiltration of Andisols in Tenerife (Canary Islands, Spain). Catena. 98, 55–62. https://doi.org/10.1016/j.catena.2012.06.006

Niu, C.Y., Shi Y.F., Fan, G.Q., et al., 2023. Effect of Rock Fragments on Soil Water and Nutrient: a Case Study in Rocky Mountain Area of North China. J SOIL SCI PLANT NUT, 24(1), 716-731. https://doi.org/ 10.1007/S42729-023-01578-9.

Noellemeyer, E., Frank, F., Alvarez, C., et al., 2008. Carbon contents and aggregation related to soil physical and biological properties under a land-use sequence in the semiarid region of central Argentina. Soil Tillage Res. 99(2), 179-190. https://doi.org/ 10.1016/j.still.2008.02.003

Poulenard, J., Podwojewski, P., Janeau, J.L., et al., 2001. Runoff and soil erosion under rainfall simulation of Andisols from the Ecuadorian Páramo: effect of tillage and burning. Catena. 45(3), 185–207. https://doi.org/ 10.1016/S0341-8162(01)00148-5.

Philip, J.R., 1957. The theory of infiltration: 1. The infiltration equation and its solution. Soil Sci. 83(5), 345–358. https://doi.org/10.1097/00010694-195705000- 00002.

Scholl, P., Leitner, D., Kammerer, G., et al., 2014. Root induced changes of effective 1D hydraulic properties in soil column. Plant Soil. 381(1-2), 193-213. https://doi.org/ 10.1007/s11104-014-2121-x

Silva, L.L., 2007. Fitting infiltration equations to centre-pivot irrigation data in a Mediterranean soil. Agric. Water Manag. 94(1), 83-92. https://doi.org/ 10.1016/j.agwat.2007.08.003

Sone, S.J., Oliveira, D.S.T.P., Zamboni, P.A.P., et al., 2019. Effects of Long-Term Crop-Livestock-Forestry Systems on Soil Erosion and Water Infiltration in a Brazilian Cerrado Site. Sustainability. 11(19). https://doi.org/ 10.3390/su11195339

Su, Y.Z., Yang, R., Liu, W.J., et al., 2010. Evolution of soil structure and fertility after conversion of native sandy desert soil to irrigated cropland in arid region, China. Soil Sci. 175(5), 246–254. https://doi.org/ 10.1097/SS.0b013e3181e04a2d

Sun, J., Yu, X., Wang, H., et al., 2018. Effects of forest structure on hydrological processes in China. J. Hydrol. 561, 187-199. https://doi.org/ 10.1016/j.jhydrol.2018.04.003

Taboada, M.A., Micucci, F.G., Cosentino, D.J., et al., 1998. Comparison of compaction induced by conventional and zero tillage in two soils of the Rolling Pampa of Argentina. Soil Till Res. 49(1-2), 57-63. https://doi.org/ 10.1016/s0167-1987(98)00132-9

Throop, L.H., Lajtha, K., Kramer, M. 2013. Density fractionation and ^{13}C reveal changes in soil carbon following woody encroachment in a desert ecosystem. Biogeochemistry. 112(1-3), 409-422. https://doi.org/ 10.1007/s10533-012-9735-y

Tu, Z., Chen, S., Chen, Z., et al., 2023. Hydrological Properties of Soil and Litter Layers of Four Forest Types Restored in the Gully Erosion Area of Latosol in South China. Forests. 14(2), 360. https://doi.org/10.3390/ f14020360

Umar, Farid. H., Mahmood-Khan, Z., Ahmad, I., et al., 2019. Estimation of infiltration models parameters and their comparison to simulate the onsite soil infiltration characteristics. Int. J. Agric. Biol. Eng. 12, 84–91. https://doi.org/ 10.25165/j.ijabe.20191203.4015.

Vivoni, E.R., Rinehart, A.J., Méndez-Barroso, L.A., et al., 2008. Vegetation controls on soil moisture distribution in the Valles Caldera, New Mexico, during the North American monsoon. Ecohydrology. 1(3), 225–238. https://doi.org/ 10.1002/eco.11

Vizioli, B., Cavalieri-Polizeli, K.M.V., Tormena, C.A., et al. 2021. Effects of long-term tillage systems on soil physical quality and crop yield in a Brazilian Ferralso. Soil Till Res. 209, 104935. https://doi.org/ 10.1016/J.STILL.2021.104935

Wang, L., Wang, Q., Wei, S., et al., 2008. Soil desiccation for Loess soils on natural and regrown areas. Forest Ecol Manag. 255(7), 2467–2477. https://doi.org/ 10.1016/j.foreco.2008.01.006.

Wang, H., Zhang, G.H., Liu, F., et al., 2017. Temporal variations in infiltration properties of biological crusts covered soils on the Loess Plateau of China. Catena. 159, 115–125. https://doi.org/ 10.1016/j.catena.2017.08.009\

Wang, S., Li, T., Zheng, Z., 2018a. Tea plantation age effects on soil aggregate-asSOMiated carbon and nitrogen in the hilly region of western Sichuan, China. Soil Till Res. 180, 91-98. https://doi.org/ 10.1016/j.still.2018.02.016.

Wang, F., Chen, H., Lian, J., et al., 2018b. Preferential Flow in Different Soil Architectures of a Small Karst Catchment. Vadose Zone J. 17(1), 1539-1663. https://doi.org/

10.2136/vzj2018.05.0107.

Wang, Y., Zhang, B., Lin, L., et al., 2011. Agroforestry system reduces subsurface lateral flow and nitrate loss in Jiangxi Province, China. Agric. Ecosyst. Environ. 140(3), 441-453. https://doi.org/ 10.1016/j.agee.2011.01.007

Wang, D., Liu, C., Yang, Y.S., et al., 2023. Three–dimensional pore structure characteristics of granite residual soil and their relationship with hydraulic properties under different particle gradation by X–ray computed tomography. J. Hydrol. 618, 129230. https://doi.org/10.1016/j.jhydrol.2023.129230

Watanabe, K., Kugisaki, Y., 2017. Effect of macropores on soil freezing and thawing with infiltration. Hydrological Processes. 31(2), 270-278. https://doi.org/10.1002/hyp.10939

Wilpert, K.v., 2022. Forest Soils—What's Their Peculiarity? Soil Syst. 6, 5. https://doi.org/ 10.3390/soilsystems6010005

Wu, G.L., Cui, Z., Huang, Z., 2021. Contribution of root decay process on soil infiltration capacity and soil water replenishment of planted forestland in semi-arid regions. Geoderma. 404, 115289. https://doi.org/ 10.1016/J.GEODERMA.2021.115289

Wu, G.L., Yang, Z., Cui, Z., et al., 2016a. Mixed artificial grasslands with more roots improved mine soil infiltration capacity. J. Hydrol. 535, 54–60. https://doi.org/ 10.1016/j.jhydrol.2016.01.059

Wu, G.L., Liu, Y., Fang, N.F., et al., 2016b. Soil physical properties response to grassland conversion from cropland on the semi-arid area. Ecohydrology. 9(8), 1471–1479. https://doi.org/ 10.1002/eco.1740

Wu, H., Zhang, J., Yu, L., et al., 2013. Study on water conservation capacity of litter from different types of forest in Caohai Basin. Meteorol. Environ. Res. 4(12), 17–22, 26.

Yimer, F., Messing, I., Ledin, S., et al., 2008. Effects of different land use typeson infiltration capacity in a catchment in the highlands of Ethiopia. Soil Use Manage. 24(4), 344–349. https://doi.org/ 10.1111/j.1475-2743.2008.00182.x.

Zhang, Y., Cao, F.C., Huang, L.C., et al., 2020. Comparative study and simulation of soil infiltration performance in Open Green Space. Teh Vjesn. 27(3), 812-818. https://doi.org/ 10.17559/tv-20191230171234

Zhang, G.H., Xie, Z.F., 2019. Soil surface roughness decay under different topographic conditions.

Soil Till Res. 187, 92-101. https://doi.org/ 10.1016/ j.still.2018.12.003.

Zhao, Y.G., Wu, P.T., Zhao, S.W., et al., 2013. Variation of soil infiltrability across a 79-year chronosequence of naturally restored grassland on the Loess Plateau, China. J. Hydrol. 504, 94–103. https://doi.org/ 10.1016/j.jhydrol.2013.09.039

Zheng, J. Wang, L., Zhao, J., et al., 2022. Forty-year-old orchards promote carbon storage by changing aggregate-asSOMiated enzyme activities and microbial communities. Catena. 213, 106195. https://doi.org/ 10.1016/J.CATENA.2022.106195

Zhong, X.L., Li, J.T., Li, X.J., et al., 2017. Physical protection by soil aggregates stabilizes soil organic matter under simulated N deposition in a subtropical forest of China. Geoderma. 285, 323-332. https://doi.org/ 10.1016/j.geoderma.2016.09.026

Zhu, P., Zhang, G., Wang, H., et al., 2020. Soil infiltration properties affected by typical plant communities on steep gully slopes on the Loess Plateau of China. J. Hydrol. 590, 125535. https://doi.org/ 10.1016/j.jhydrol.2020.125535

Zhu, Y., Sun, L., Jamshidi, A.H., et al., 2025. Effect of forest conversion on soil water infiltration in the Dabie mountainous area, China. J. Hydrol. Reg. Stud. 59. https://doi.org/ 10.1016/j.ejrh.2025.102351

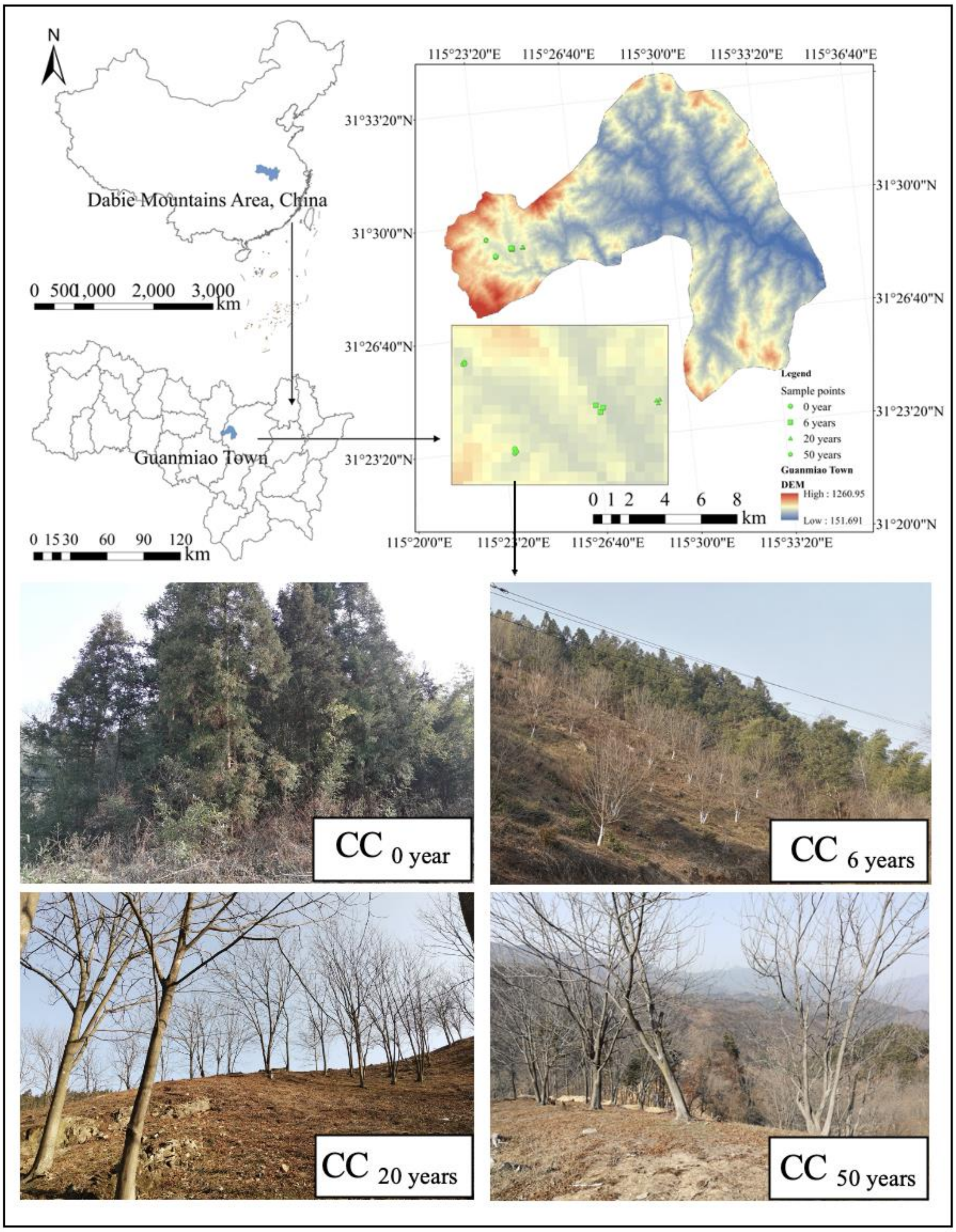

Fig. 1. The geographical location and on-site photographs of the study sites.

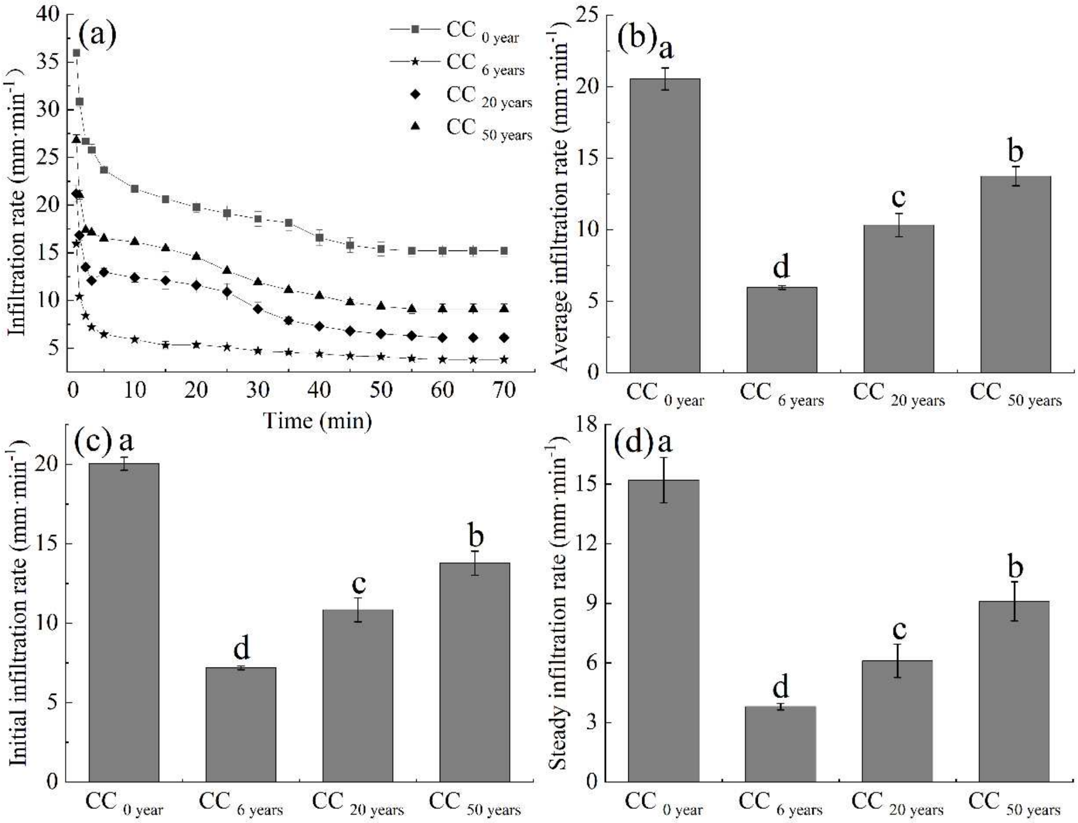

Fig. 2 Soil infiltration rate (a). *AIR*, average infiltration rate (b). *IIR*, initial infiltration rate, (c) and *SIR*, steady infiltration rate, (d) under different treatments. Different lowercase letters represent statistical significance at 0.05 level.

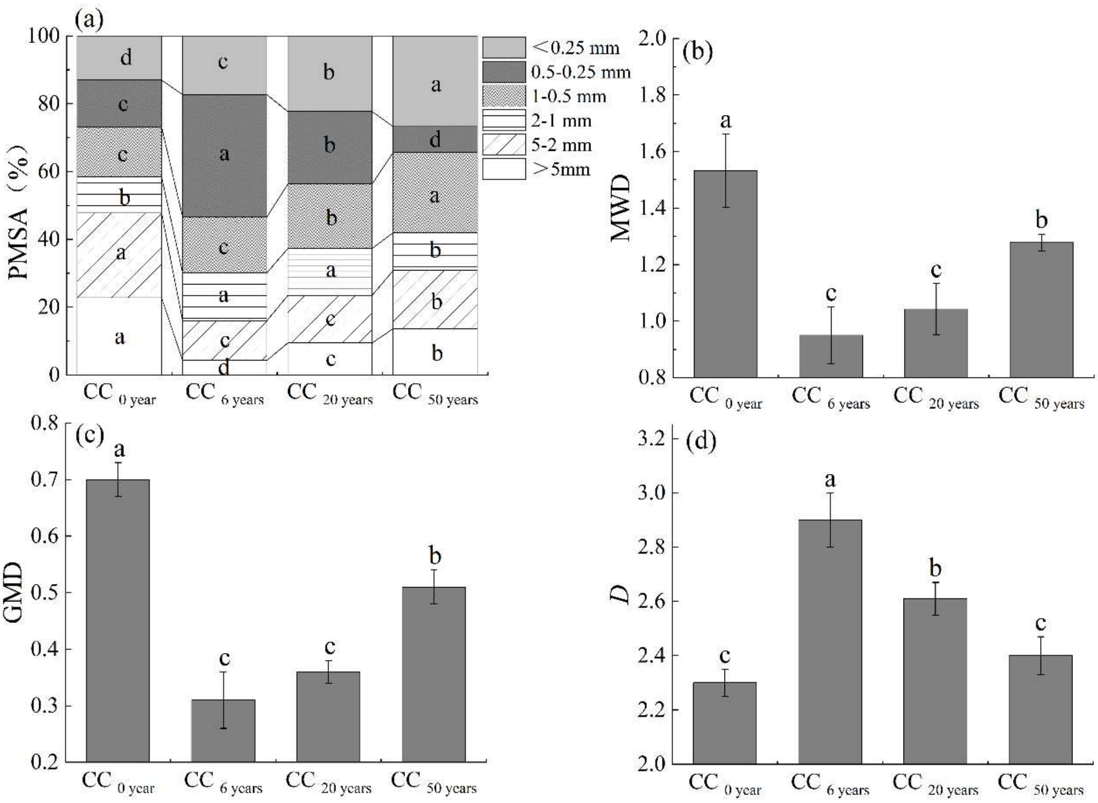

Fig. 3 PMSA, percentage of mechanical stable aggregates (a). MWD, soil mean weight diameter, (b). GMD, soil geometric mean diameter, (c) and *D*, soil fractal dimension (d) of mechanical stable aggregate fractions. Different lowercase letters represent statistical differences at 0.05 level.

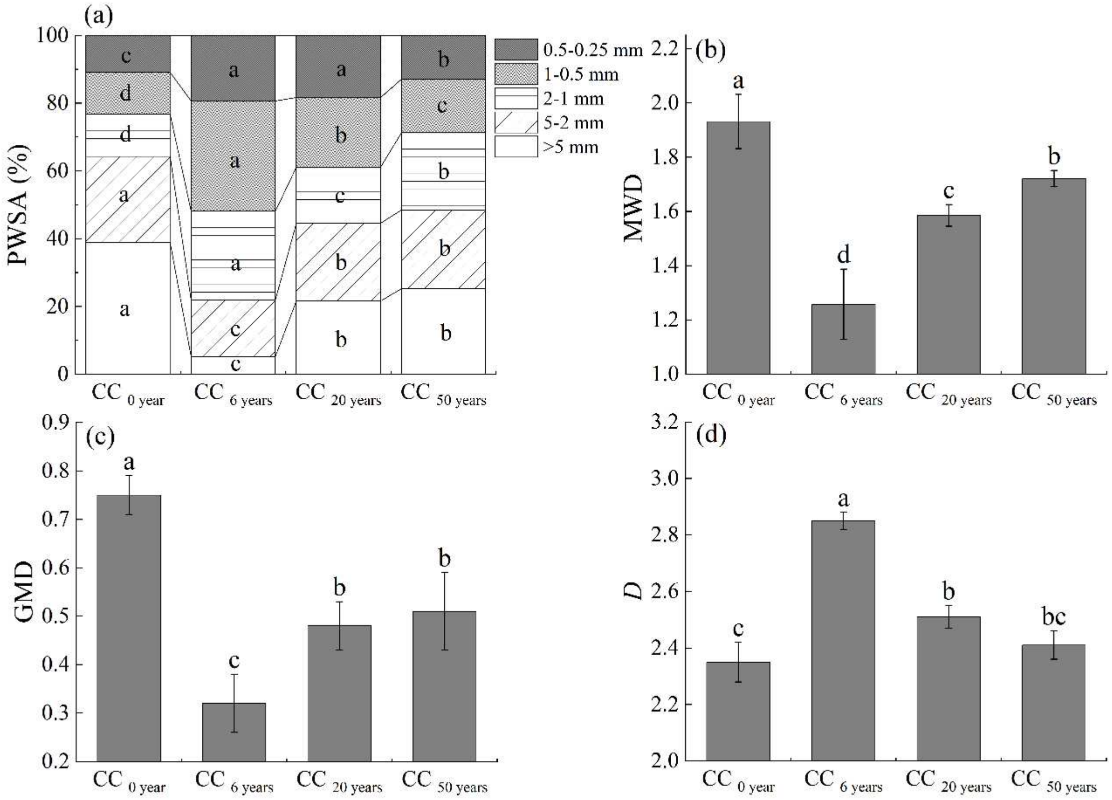

Fig. 4 PWSA, percentage of water stable aggregates, (a). MWD, soil mean weight diameter, (b). GMD, soil geometric mean diameter, (c). *D*, soil fractal dimension (d) of water stable aggregate fractions. Different lowercase letters represent statistical differences at 0.05 level.

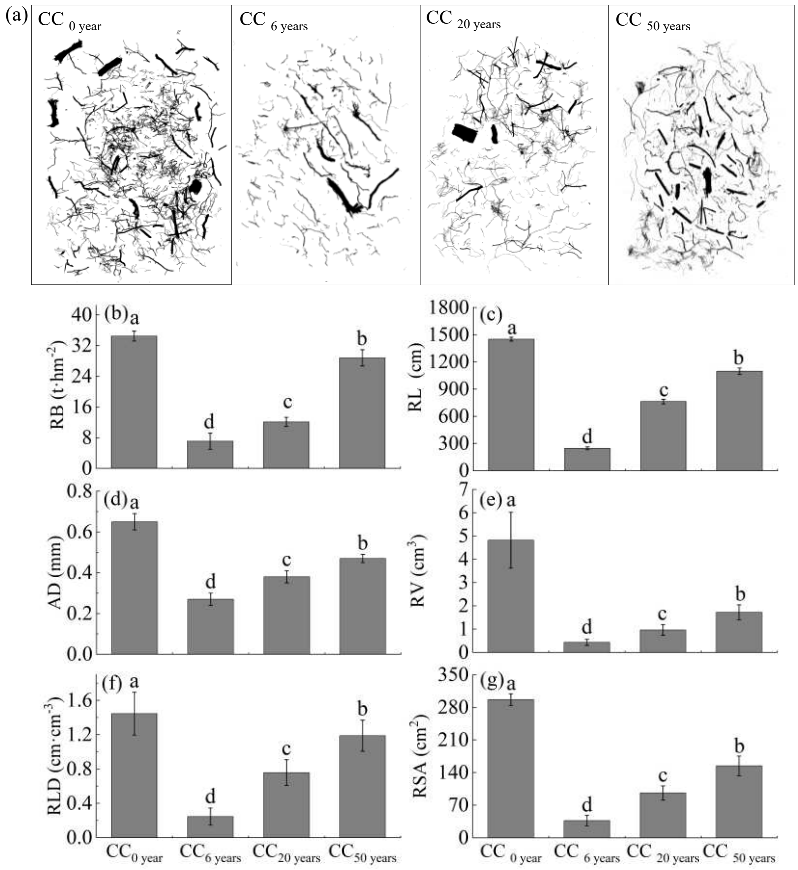

Fig. 5 The imaged of plant root distribution (a). RB, root biomass (b). RL, root length (c). AD, average diameter (d). RV, root volume (e). RLD, root length density (f). RSA, root surface area (g) in 0-20 cm soil depth under different treatment. Different lowercase letters represent statistical differences at 0.05 level.

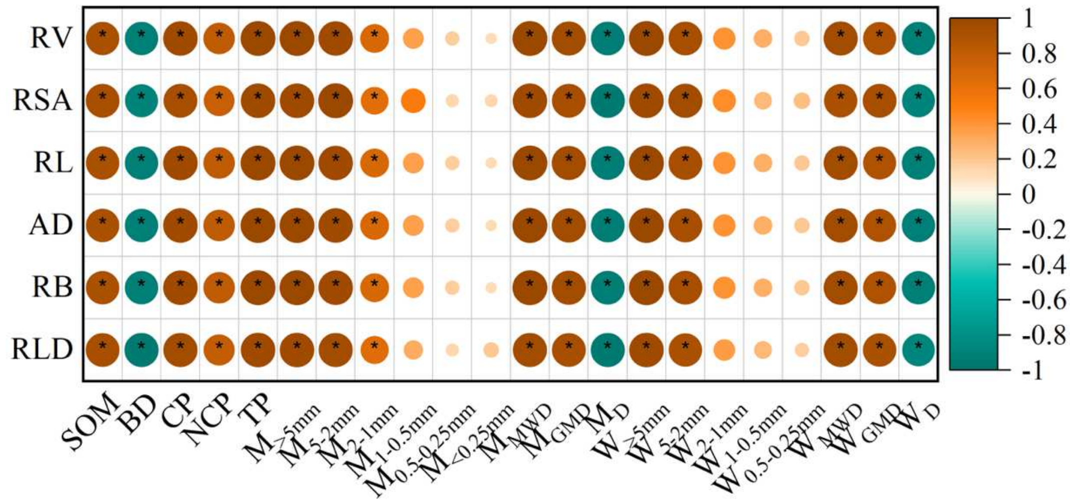

Fig. 6. Correlation coefficients between soil properties and root morphological traits. SOM, soil organic matter; BD, bulk density; CP, capillary porosity; NCP, Non-capillary porosity; TP, total porosity; $M_{>5mm}$, mechanical aggregate >5mm; $M_{5\text{-}2mm}$, mechanical aggregate 5-2mm; $M_{2\text{-}1mm}$, mechanical aggregate 2-1mm; $M_{1\text{-}0.5mm}$, mechanical aggregate 2-1mm; $M_{0.5\text{-}0.25mm}$, mechanical aggregate 0.5-0.25mm; M_D, mechanical aggregate fractal dimension; M_{MWD}, mechanical aggregate mean weight diameter; M_{GMD}, mechanical aggregate geometric mean diameter; $W_{>5mm}$, water aggregate >5mm; $W_{5\text{-}2mm}$, water aggregate 5-2mm; $W_{2\text{-}1mm}$, water aggregate 2-1mm; $W_{1\text{-}0.5mm}$, water aggregate 1-0.5mm; $W_{0.5\text{-}0.25mm}$, water aggregate 0.5-0.25mm; W_{MWD}, water aggregate mean weight diameter; W_{GMD}, water aggregate geometric mean diameter; W_D, water aggregate fractal dimension; RV, root volume; RSA, root surface area; RL, root length; RB, root biomass; AD, average diameter; RLD, root length density. Circle size indicates the magnitude of the correlation coefficient.

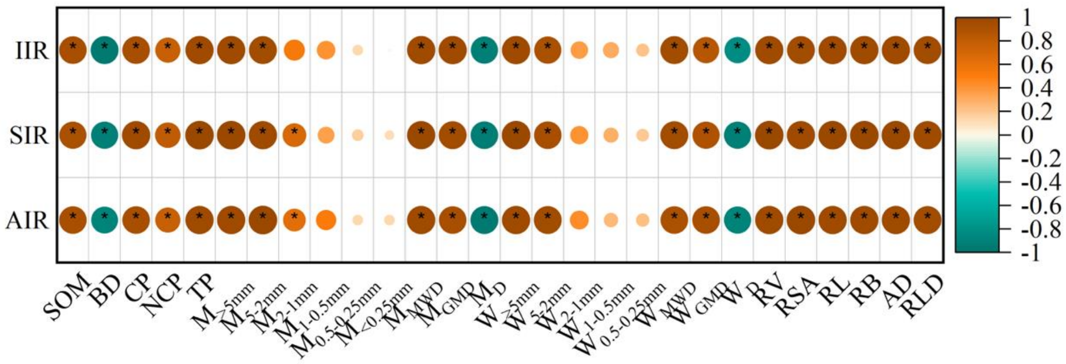

Fig. 7. Correlation coefficients between soil infiltration characteristics (*IIR*, initial infiltration rate; *SIR*, stable infiltration rate; *AIR*, average infiltration rate), soil properties, and root morphological traits. SOM, soil organic matter; BD, bulk density; CP, capillary porosity; NCP, non-capillary porosity; TP, total porosity; $M_{>5mm}$, mechanical aggregate >5mm; $M_{5\text{-}2mm}$, mechanical aggregate 5-2mm; $M_{2\text{-}1mm}$, mechanical aggregate 2-1mm; $M_{1\text{-}0.5mm}$, mechanical aggregate 2-1mm; $M_{0.5\text{-}0.25mm}$, mechanical aggregate 0.5-0.25mm; M_D, mechanical aggregate fractal dimension; M_{MWD}, mechanical aggregate mean weight diameter; M_{GMD}, mechanical aggregate geometric mean diameter; $W_{>5mm}$, water aggregate >5mm; $W_{5\text{-}2mm}$, water aggregate 5-2mm; $W_{2\text{-}1mm}$, water aggregate 2-1mm; $W_{1\text{-}0.5mm}$, water aggregate 1-0.5mm; $W_{0.5\text{-}0.25mm}$, water aggregate 0.5-0.25mm; W_{MWD}, water aggregate mean weight diameter; W_{GMD}, water aggregate geometric mean diameter; W_D, water aggregate fractal dimension; RV, root volume; RSA, root surface area; RL, root length; RB, root biomass; AD, average diameter; RLD, root length density. Circle size indicates the magnitude of the correlation coefficient.

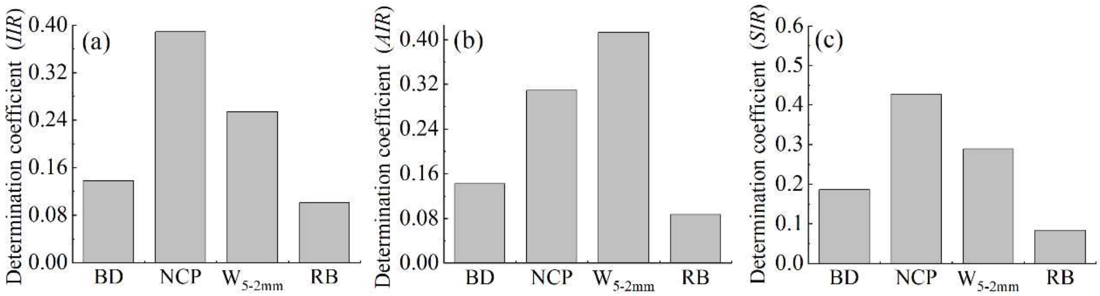

Fig. 8 The determination coefficients of BD, NCP, $W_{5\text{-}2mm}$ and RB on *IIR* (a), *AIR* (b) and *SIR* (c). BD, bulk density; NCP, non-capillary porosity; $W_{5\text{-}2mm}$, water aggregate 5-2mm; RB, root biomass; *IIR*, initial infiltration rate; *SIR*, stable infiltration rate; *AIR*, average infiltration rate.

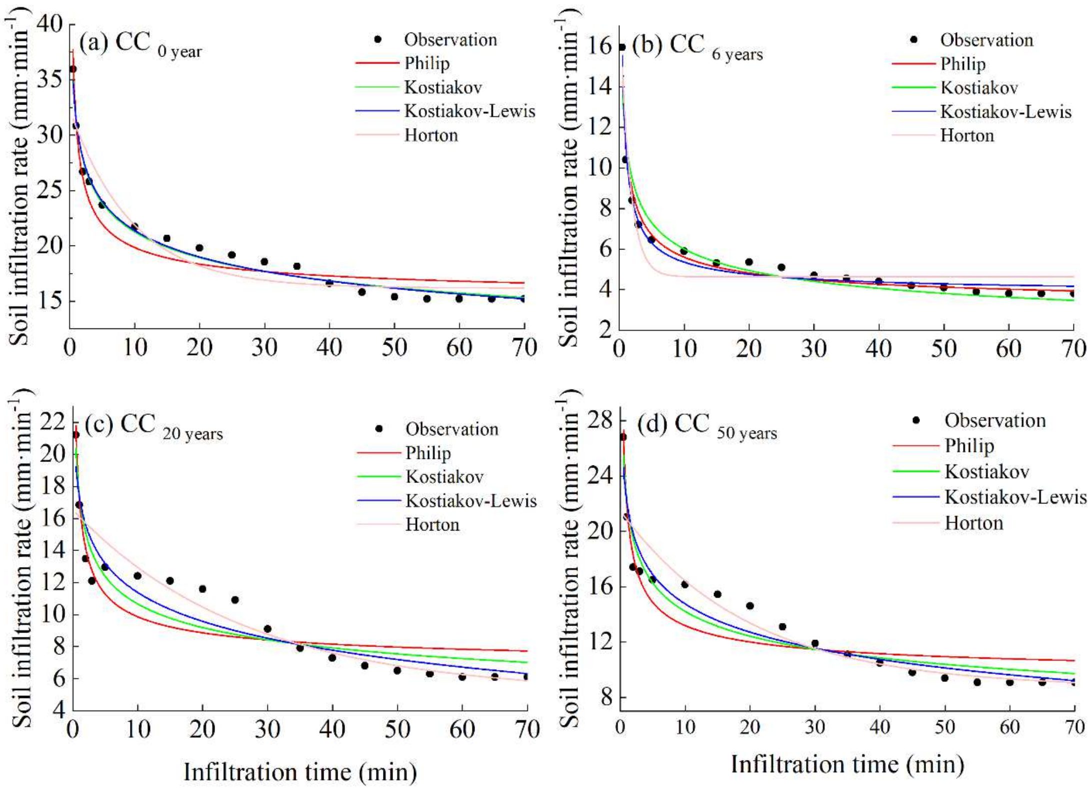

Fig.9 The comparison diagram of soil infiltration processes of different planting years by different infiltration models was obtained. (a), $CC_{0\ year}$. (b), $CC_{6\ years}$. (c), $CC_{20\ years}$. (d), $CC_{50\ years}$.

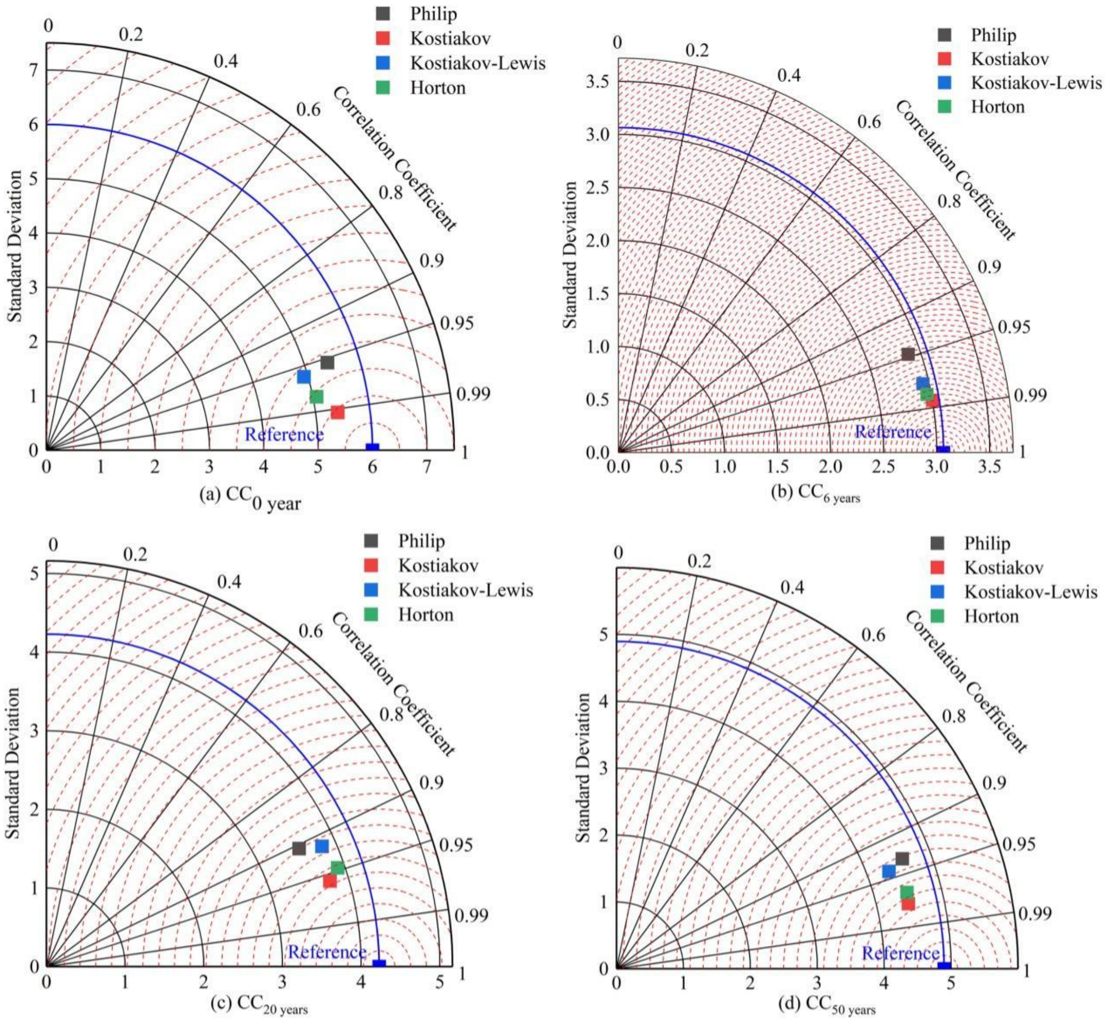

Fig. 10 Taylor program for infiltration rates among infiltration models with observations. (a), CC $_{0\ year}$. (b), CC $_{6\ years}$. (c), CC $_{20\ years}$. (d), CC $_{50\ years}$. The scattered points in the Taylor diagram represent the model, the radial lines represent the correlation coefficient, the horizontal and vertical axes represent the standard deviation, and the dotted line represents the root mean square error.

Table 1. the detailed information of sampling sites under different planting years

Planting years	Slope grade(°)	Slope aspect	Slope position	Altitude (m)	Tree height (m)	Crown width (m)	Row and plant spacing (m)	Diameter at breast height (cm)	Canopy (%)	Litter coverage (%)
$CC_{0\ year}$	25	North-east	Down	400-600	NA	NA	NA	NA	40	100
$CC_{6\ years}$	37	North	Down	200-400	3.5	3×3.5	10×6	30	20	95
$CC_{20\ years}$	32	North	Down	200-400	4.2	7×7.5	10×10	60	25	100
$CC_{50\ years}$	20	North-west	Up	600-800	9	7×9.5	6×6	75	15	90

Table 2. Basic soil properties under under different treatments.

Planting years	SOM ($g·kg^{-1}$)	BD ($mg·m^{-3}$)	CP (%)	NCP (%)	TP (%)
CC $_{\text{0 year}}$0	21.66±1.27 b	0.95±0.07 d	43.02±3.42 a	13.10±1.88 a	56.12±1.54 a
CC $_{\text{6 years}}$6	15.50±2.55 c	1.52±0.12 a	25.56±1.74 d	6.66±0.60 b	32.22±1.14 d
CC $_{\text{20 years}}$20	35.91±3.93 a	1.31±0.06 b	32.68±0.12 c	5.44±1.65 b	38.12±1.53 c
CC $_{\text{50 years}}$50	26.10±1.83 b	1.16±0.08 c	38.12±0.61 b	8.40±1.56 b	46.52±1.96 b

Note: SOM, soil organic matter; BD, bulk density; CP, capillary porosity; NCP, non-capillary porosity; TP, total porosity. Different lowercase letters represent statistical differences at 0.05 level.

Table 3. Regression equation of soil infiltration rates and influncing factors.

	Kolmogorov-Smirnova			*Shapiro-Wilk*			Stepwise Multiple Regression	R^2
	Statistics	d*f*	*P*	Statistics	d*f*	*P*	Equation	
IIR	0.151	12	0.200*	0.910	12	0.219	Y_1=-3.341–2.873 BD + 0.879 NCP +0.629 $W_{5\text{-}2mm}$ – 0.062 RB	0.989
AIR	0.150	12	0.200*	0.917	12	0.328	Y_2=-19.584+4.683 BD +1.298 NCP +0.874 $W_{5\text{-}2mm}$ + 0.182 RB	0.967
SIR	0.153	12	0.200*	0.923	12	0.293	Y_3=-20.872+4.032 BD +1.302 NCP +0.529 $W_{5\text{-}2mm}$ +0.206 RB	0.984

Note: *IIR*, initial infiltration rate; *AIR*, average infiltration rate; *SIR*, stable infiltration rate; BD, bulk density; NCP, non-capillary porosity; $W_{5\text{-}2mm}$, water aggregate 5-2 mm; RB, root biomass. * represents a significant correlation at the $p = 0.05$ level.

Table 4. Path coefficients between environmental factors and soil infiltration characteristics.

Soil infiltration characteristics	Independent Variable	Correlation Coefficient	Direct Path Coefficient	Indirect Path Coefficients				
				BD	NCP	$W_{5\text{-}2mm}$	RB	Total
IIR	BD	-0.941	-0.181	/	-0.598	-0.353	0.191	-0.760
	NCP	0.895	0.521	0.156	/	0.298	-0.080	0.374
	$W_{5\text{-}2mm}$	0.828	0.389	0.186	0.342	/	-0.089	0.439
	RB	0.905	0.169	0.138	0.233	0.365	/	0.736
AIR	BD	-0.932	-0.214	/	-0.435	-0.346	-0.063	-0.718
	NCP	0.907	0.608	-0.064	/	0.312	0.051	0.299
	$W_{5\text{-}2mm}$	0.872	0.583	-0.080	0.341	/	0.028	0.289
	RB	0.951	0.126	-0.178	0.518	0.485	/	0.825
SIR	BD	-0.916	-0.201	/	-0.608	-0.412	-0.097	-1.117
	NCP	0.923	0.759	-0.148	/	0.287	0.025	0.164
	$W_{5\text{-}2mm}$	0.805	0.314	-0.176	0.552	/	0.115	0.491
	RB	0.945	0.102	-0.231	0.573	0.501	/	0.843

Note: *IIR*, initial infiltration rate; *AIR*, average infiltration rate; *SIR*, stable infiltration rate; BD, bulk density; NCP, non-capillary porosity; $W_{5\text{-}2mm}$, water aggregate 5-2 mm; RB, root biomass.

Table 5 Fitting and accuracy evaluation of soil infiltration models under different planting years

Soil infiltration models	Parameters	CC $_{0\ year}$	CC 6 years	CC $_{20\ years}$	CC $_{50\ years}$
Philip	*m*	32.578	16.949	21.725	25.778
	n	14.697	2.924	6.429	9.116
	R^2	0.942	0.977	0.844	0.885
Kostiakov	*α*	31.340	11.523	17.532	22.287
	b	0.168	0.283	0.216	0.195
	R^2	0.986	0.940	0.911	0.930
Kostiakov-lewis	*α*	35.390	7.499	21.076	59.932
	n	0.143	0.658	0.125	0.057
	b	-4.069	3.709	-5.453	-37.740
	R^2	0.930	0.984	0.905	0.935
Horton	*p*	32.298	19.006	16.550	21.506
	q	16.166	4.625	5.048	8.705
	k	-0.103	-0.663	-0.038	-0.050
	R^2	0.914	0.927	0.847	0.866